

# Solar sail with inflatable toroidal shell

V. Ya. Kezerashvili<sup>1</sup>, R. Ya. Kezerashvili<sup>1,2</sup>, O. L. Starinova<sup>3</sup>

<sup>1</sup>*Physics Department, New York City College of Technology, The City University of New York,  
Brooklyn, NY 11201, USA*

<sup>2</sup>*The Graduate School and University Center, The City University of New York, New York, NY 10016, USA*

<sup>3</sup>*Samara National Research University, Russian Federation, Samara, Russia*

(Dated: August 17, 2022)

In the framework of a strict mathematical approach based on classical theory of elasticity we present an idea of the deployment and stretching of the circular solar sail attached to the inflatable toroidal shell. It is predicted that by introducing the gas into the inflatable toroidal shell one can deploy and stretch a large size circular solar sail membrane. The formulas for the toroidal shell and sail membrane stresses and strains caused by the gas pressure in the shell are derived. The analytical expressions can be applied to a wide range of solar sail sizes. Numerical calculations for the sail of radii up to 100 m made of CP1 membrane and attached to the toroidal shell with the varied cross-section radius are presented. The normal transverse vibration modes of the sail membrane under tension caused by gas pressure in the shell are calculated. The feasibility of deployment and stretching of a solar sail with a large size circular membrane attached to the inflatable toroidal shell is demonstrated.

## I. INTRODUCTION

Currently the main space exploration vehicle relies on chemical propulsion system and most missions provide energy by means of prelaunch onboard fuel. A solar sail is propellant-less propulsion system for space exploration that uses the Sun radiation as a propulsion mechanism. A solar sail is a large sheet of low areal density material that gains an acceleration due to the reflection and absorption of the Sun electromagnetic flux [1–4]. The proposals to use solar sails cover almost the whole spectrum of space missions, from an expedition to Mars to scientific probes, from continuous planetary polar observation to mining exploitation of the asteroids, even implementations for deep space exploration and interstellar travel are considered. The successful deployment of the world's first interplanetary solar sail IKAROS, NASA's first solar NanoSail-D and the Interplanetary Society solar sail LightSail-2 demonstrates the feasibility of exploration of the Solar system by means of the electromagnetic radiation pressure.

Studies on a solar sail have four primary foci: i. finding low areal density material that allows to utilize the maximum acceleration due to the solar radiation pressure; ii. missions design for exploration of the Solar System and beyond using the solar sail; iii. maximizing the solar thrust through the increase of area of the solar sail made of a low areal density material; iv. the development of the mechanism for the deployment and stretching the large size of solar sail membrane. In this work we concentrated on the last two objectives.

The sail's membrane deployment strategies has attracted considerable attention. Many different systems have been previously considered for the sails opening. The deployment is usually performed: by uniaxial mechanisms, such as the telescopic, deployable and inflatable booms; the extendable masts; the centrifugal force that renders a spin-type deployment mechanism; by the presence of guide rollers; electromechanical actuation devices, or composite booms; the solar sail self-deployment based on shape memory alloys, (see Refs. [5–16] and references therein) and most recently the deployment of the large size solar sail was considered using the superconducting current-carrying wire [17, 18]. We cite these works, but the recent literature on the subject is not limited by them. It is worth mentioning that in the actual deployment technology, the main limit is still the high weight of the system and the complexity of the deployment mechanism for solar sail surface.

The concept of using inflatable structures for a spacecraft has been extensively discussed during the past six decades. In the 1960s NASA launched the Echo balloons that were some of the first inflatable structures to be utilized in space [19]. Once such a structure is inflated and deployed, it operates by similar to rigid structures principles and allows to obtain comparable or greater performance. The advantages of inflatable structures are a simple deployment mechanism for large space structures, the small mass and space savings in the launch configuration [20].

Inflatable structures have the characteristics that are particularly advantageous for a solar sail: i. extremely lightweight that is critical for a solar sail; ii. a simple mechanism to deploy it in orbit.

The use of inflatable structures for solar sailing goes back to 1989 when Strobl [21] proposed a hydrogen inflated hollow disk-shaped sail with a molybdenum reflector. Later the idea of the inflatable ring sail was presented in Ref. [22]. Inflatable structures including the solar sail have been the subject of interest in the past and recent years and investigated in Refs. [6, 10, 24–30]. Most recently a sail consisting of a reflective membrane attached to an inflatable torus-shaped shell was suggested [30]. The sail deployment from its stowed configuration is initiated by introduction of the inflation pressure into the toroidal shell. However, the study [30], as well as the previous investigations did not address important issues related to the elastic properties of the sail membrane and torus-shaped shell. The toroidal shell is kept pressurized by the gas after deployment, withholds all the stresses, and allows a very simple straightforward deployment procedure of a large area circular configuration.

In this work we consider the toroidal shell that is attached to a circular solar sail membrane to aid the membrane deployment and stretching. The sail’s deployment from its stowed configuration is initiated by introducing inflation pressure into the toroidal shell. We provide the rigorous consideration of this system within the framework of the classical theory of elasticity [31, 32]. An important question that arises in the context of deployable toroidal-shaped solar sail is its mass and stability. We consider statics of a deployed torus-shaped sail, and address the structural strength of the sail membrane and inflated toroidal shell to support the flat surface of a circular membrane. The governing equation for a gas in an inflated toroidal shell is assumed to be the equation for a real gas. Within such approach we investigate the effects of both the enclosed gas pressure and structure stiffness and the stability of the solar sail. It is demonstrated that the effect of the enclosed gas must be considered in the analysis of the inflatable torus with the membrane.

This article is organized in the following way. In Sec. II we consider the solar sail configuration and within the framework of the classical theory of elasticity derive the forces that lead to the deployment of a circular sail membrane attached to the toroidal shell. The stress and strain of the toroidal shell, the circular membrane and the toroidal shell-membrane structure are addressed. The vibration of the deployed and stretched membrane are considered in Sec. III. Results of the numerical calculations and discussion are presented in Sec. IV. The conclusions follow in Sec. V.

## II. SOLAR SAIL AS A CIRCULAR MEMBRANE ATTACHED TO A TOROIDAL SHELL

A schematic of the circular solar sail attached to a torus of radius  $R$  and a circular cross-section of radius  $r$  inflated by a gas is presented in Fig. 1. The radius of the toroidal shell is significantly greater than the radius cross-section:  $R \gg r$ . The solar sail membrane is stretched by forces generated by pressure of the gas introduced into the toroidal shell. In this Section we consider the strain in a toroidal shell due to the gas pressure and provide the detailed consideration of the stress and strain in the circular membrane resulting from uniformly distributed force applied to the membrane edge and caused by the gas pressure. Finally, the system of the toroidal shell filled by the gas attached to the sail’s circular membrane is considered.

### A. Toroidal shell filled with gas

A key component and basic structural element of the torus-shaped solar sail is a toroidal shell. The gas filled toroidal shell attached to the circular membrane (Fig. 1a) provides structural support to the sail. Here we consider a static behavior of an inflated toroidal shell following Ref. [33]. We assume large aspect ratio,  $\frac{R}{r} \gg 1$ . Therefore,  $R \gg r$  and it is a very reasonable approximation to consider that the radius of the circular sail membrane  $R - r \simeq R$  is the radius of the torus. Also the thickness of the torus shell  $t_t$  is negligible compared to the radii of curvature.

An implicit equation for a torus with a large aspect ratio that is azimuthally symmetric about the  $z$ -axis in Cartesian coordinates is

$$(R - \sqrt{x^2 + y^2})^2 + z^2 = r^2, \quad (1)$$

where  $R$  is the distance from the center of the toroidal shell to the center of the torus and  $r$  is the radius of the toroidal shell as is shown in Fig. 1b. This torus is generated by revolving the circle  $(x - R)^2 + z^2 = r^2$  of radius  $r$  in the  $x - z$  plane about the  $z$  axis at the distance  $R$  from the center of the circle.

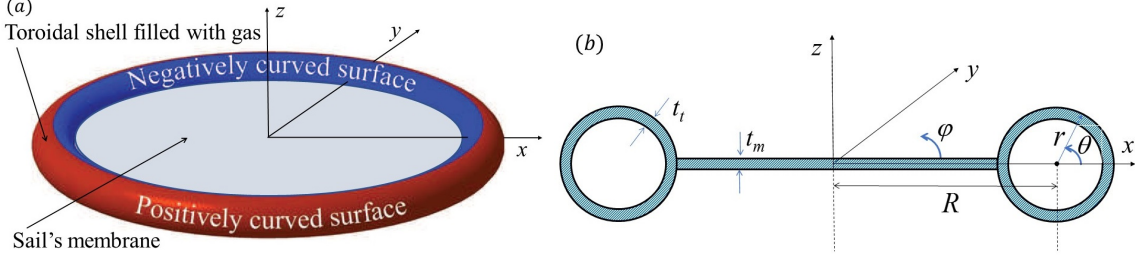


FIG. 1: (Color online) (a) Torus-shaped solar sail and its geometric characteristics. (b)  $R$  and  $r$  are the radii of the torus and the toroidal shell cross-section, respectively. Throughout of this work we assume that the radius of the torus is much greater than the radius of the toroidal shell:  $R \gg r$ .  $t_m$  and  $t_t$  are the thicknesses of the sail membrane and toroidal shell, respectively.

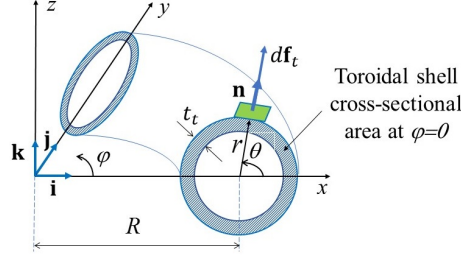


FIG. 2: (Color online) A schematic of the element of the toroidal shell inflated by the gas. The force  $df_t$  acts on the surface element of the shell at the angle  $\theta$  per unit of the length of toroidal ring at the angle  $\varphi = 0$ . The radius  $R$  is much greater than the cross-section radius of the torus  $r$ :  $R \gg r$ . The figure is not to scale.

In our consideration it is convenient to use toroidal and poloidal coordinates for description of the torus geometry: the polar coordinate  $(r, \theta)$  for each cross-section and toroidal coordinate  $\varphi$  around the toroidal ring. The three coordinate  $r, \theta, \varphi$  ( $\theta \in [0, 2\pi]$ ,  $\varphi \in [0, 2\pi]$ ) of curved coordinate system are orthogonal to each other. The toroidal coordinate is used to describe those quantities along the direction normal to the cross-section, while the poloidal coordinates are used to describe an interior of the toroidal shell. The toroidal and poloidal coordinate system relates to standard Cartesian coordinates as follows

$$\begin{aligned} x &= (R + r \cos \theta) \cos \varphi, \\ y &= (R + r \cos \theta) \sin \varphi, \\ z &= r \sin \theta. \end{aligned} \quad (2)$$

Of our special interest are the forces that act on the surface area of the torus. The total surface area of the torus can be considered as a sum of the outer and inner surfaces as shown in Fig. 1a. The outer surface is a positively curved in a contrast of the inner surface, which is negatively curved. It is obvious that the outer surface is larger than the inner one and the difference in surface area is  $\Delta A = 8\pi r^2$ . Therefore, the pressure of the gas  $P$  in toroidal shell filled with the gas produces the larger force on the outer surface of the shell than on the inner one. Let us find the net force due to the gas pressure  $P$  in the toroidal shell that keeps the torus inflated. We consider the torus circular cross-section at the angle  $\varphi = 0$  as it is depicted in Fig. 2. The differential of the force  $d\mathbf{f}_t$  acting on the surface element  $dA$  at angle  $\theta$  per unit of the length of toroidal ring  $Rd\varphi$  is  $d\mathbf{f}_t = \frac{PdA\hat{\mathbf{n}}}{Rd\varphi}$ , where  $dA = (R + r \cos \theta)d\varphi r d\theta$  and  $\hat{\mathbf{n}} = \cos \theta \mathbf{i} + \sin \theta \mathbf{k}$  is a unit vector normal to the surface element  $dA$  with the unit vectors  $\mathbf{i}$  and  $\mathbf{k}$  along  $x$  and  $y$  axis, respectively. Therefore, the net force that acting on the unit length of the toroidal shell at  $\varphi = 0$  is

$$\mathbf{F}_t = \int_0^{2\pi} \frac{P}{R} (R + r \cos \theta) (\cos \theta \mathbf{i} + \sin \theta \mathbf{k}) r d\theta = \frac{\pi P r^2}{R} \mathbf{i}. \quad (3)$$

The force  $\mathbf{F}_t$  is directed along  $x$  axis radially out of the torus center, which is expected due to the mirror symmetry of the torus with respect of the  $x - y$  plane. The magnitude of the force  $\mathbf{F}_t$  at  $\varphi = 0$  acting

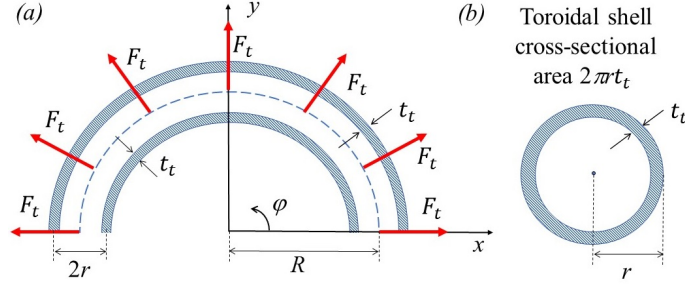


FIG. 3: (Color online) (a) Schematics for the action of uniform radial forces  $F_t$  per unit of circumferential length on the toroidal shell. (b) The area of the toroidal shell cross-section is  $A = 2\pi r t_t$ . The figure is not to scale:  $R \gg r$  and  $r \gg t_t$

on the unit length of the toroidal shell is

$$F_t = \frac{\pi P r^2}{R}. \quad (4)$$

Due to the fact that the  $z$ -axis is the axis of rotational symmetry of infinite order the magnitude of the force  $F_t$  for any toroidal angle  $\varphi \in [0, 2\pi]$  is the same as (4) for  $\varphi = 0$  and is directed radially out as shown in Fig. 3. This force is responsible for the tensile stress  $\sigma_t$  of the toroidal shell resulting in tensile strain  $\Delta R_t/R$ .

The net force acting on the toroidal shell cross-section of the area  $2\pi r t_t$  is  $\frac{1}{2} \int_0^\pi F_t \sin \varphi R d\varphi = F_t R$ . In the limit of the linear response one can apply the Hook's law and obtains the tensile stress in the toroidal shell [31]

$$\sigma_t = \frac{F_t R}{2\pi r t_t} = E_t \frac{\Delta R_t}{R}. \quad (5)$$

In Eq. (5)  $E_t$  and  $t_t$  are Young's modulus and the thickness of the toroidal shell material, respectively. From Eq. (5) we get for the strain and  $\Delta R_t$  the following expression:

$$\frac{\Delta R_t}{R} = \frac{F_t R}{2\pi E_t r t_t}, \quad (6)$$

$$\Delta R_t = \frac{F_t R^2}{2\pi E_t r t_t}. \quad (7)$$

This  $\Delta R_t$  is for a stand-alone torus. In the equilibrium of the stand-alone gas filled torus under the force  $F_t$  is balanced by the opposite elastic forces.

The toroidal shell is made from a material with density  $\rho_t$  and the density of the material of the membrane is  $\rho_m$ . The thicknesses of the foil for the toroidal shell and membrane are  $t_t$  and  $t_m$ , respectively. Thus, the mass of the sail is

$$M = \pi \rho_m R^2 t_m + 4\pi^2 \rho_t r R t_t + M_g, \quad (8)$$

where  $M_g$  is the mass of the gas.

## B. Stress and strain of circular membrane

Ideally the torus-shaped solar sail has the attached membrane of the radius  $R - r$ . However, as we mentioned before for the torus-shaped sail with large aspect ratio when  $R \gg r$ , the radius of the membrane can be considered as  $R$ . Consider a thin circular membrane of the radius  $R$  and thickness  $t_m$  ( $t_m \ll R$ ) under a uniform distributed force  $F_m$  per unit length of a circumference acting at the membrane edge in the radial direction as shown in Fig. 4. If the membrane is sufficiently thin, the deformation can be

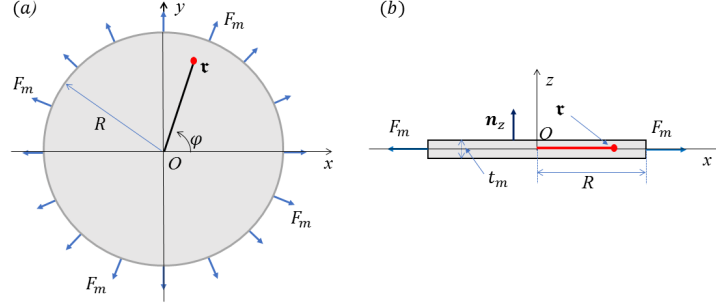


FIG. 4: (Color online) Schematics for the action of the uniformly distributed radial force  $F_m$  per unit of circumferential length of the circular membrane: (a) top view; (b) side view. The figure is not to scale:  $R \gg t_m$

treated as uniform over its thickness and we have to deal with longitudinal deformations of the membrane and not with any membrane bending. For a two-dimensional case the strain tensor is a function of  $x$  and  $y$  coordinates and is independent on  $z$ . The boundary conditions for the stress tensor on both surfaces of the membrane are [32]

$$\sigma_{ik}n_k = 0, n_k = n_z, i = x, y, z, \quad (9)$$

where  $\mathbf{n}_z$  is the normal vector parallel to  $z$ -axis, and lead to

$$\sigma_{xz} = \sigma_{yz} = \sigma_{zz} = 0 \quad (10)$$

in the entire volume of the membrane when  $t_m \ll R$  [32].

The equation of equilibrium in the absence of the body forces in the two-dimensional vector form is [32]:

$$\text{grad div } \mathbf{u} - \frac{1}{2}(1 - \nu_m)\text{curl curl } \mathbf{u} = 0, \quad (11)$$

where  $\mathbf{u}$  is the displacement vector,  $\nu_m$  is the membrane Poisson ratio and the vector operators *grad*, *div* and *curl* are two-dimensional. Due to the axial symmetry  $\mathbf{u}$  is directed along the radius and is a function of  $r$  only, so  $\text{curl } \mathbf{u} = 0$  and Eq. (11) in polar coordinates becomes:

$$\text{div } \mathbf{u} = \frac{1}{r} \frac{d(ru)}{dr} = \text{const} \equiv 2c \quad (12)$$

and gives

$$u = cr + \frac{d}{r}. \quad (13)$$

Therefore, the stress tensor radial and angular components are

$$u_{rr} = \frac{du}{dr} = c - \frac{d}{r^2}, \quad u_{\varphi\varphi} = \frac{u}{r} = c + \frac{d}{r^2}, \quad (14)$$

where in (14)  $c$  and  $d$  are some constants [34]. In polar coordinates at  $\varphi = 0$  the stress  $\sigma_{ik}$  and strain  $u_{ik}$  tensor components are:

$$\sigma_{rr} = \sigma_{xx}, \quad \sigma_{\varphi\varphi} = \sigma_{yy}, \quad (15)$$

$$u_{rr} = u_{xx}, \quad u_{\varphi\varphi} = u_{yy}. \quad (16)$$

The general equations relating the strain tensor components to the stress tensor components [32] in our case when  $\sigma_{zz} = 0$  become:

$$\sigma_{xx} = \frac{E_m}{1 - \nu_m^2} (u_{xx} + \nu_m u_{yy}), \quad (17)$$

$$\sigma_{yy} = \frac{E_m}{1 - \nu_m^2} (u_{yy} + \nu_m u_{xx}), \quad (18)$$

where  $E_m$  and  $\nu_m$  are the Young modulus of elasticity and Poisson ratio of the membrane, respectively. By substituting (15) and (16) at  $\varphi = 0$  into (17) and (18) the stress tensor radial and angular components become:

$$\sigma_{rr} = \frac{E_m}{1 - \nu_m^2} (u_{rr} + \nu_m u_{\varphi\varphi}), \quad (19)$$

$$\sigma_{\varphi\varphi} = \frac{E_m}{1 - \nu_m^2} (u_{\varphi\varphi} + \nu_m u_{rr}). \quad (20)$$

The requirement for the deformation  $u$  (14) to be finite at the membrane center and the boundary condition for  $\sigma_{rr}$  (19) combined with  $u_{rr}$  and  $u_{\varphi\varphi}$  (14) at the membrane edge:

$$u(0) = 0 \text{ and } \sigma_{rr}(r = R) = \frac{F_m}{t_m} \quad (21)$$

determine the values of the constants  $c$  and  $d$ :

$$c = \frac{F_m (1 - \nu_m)}{t_m E_m}, \quad d = 0. \quad (22)$$

The use of the constants (22) allows to obtain the expressions for the deformation vector  $\mathbf{u}$  (13) and the strain (14), as well as the stress tensor components (19), (20):

$$\mathbf{u} = \frac{F_m (1 - \nu_m)}{t_m E_m} \mathbf{r}, \quad (23)$$

$$u_{rr} = u_{\varphi\varphi} = \frac{F_m (1 - \nu_m)}{t_m E_m}, \quad (24)$$

$$\sigma_{rr} = \sigma_{\varphi\varphi} = \frac{F_m}{t_m}. \quad (25)$$

As expected the stress distribution (25) in the membrane deformed by the forces acting at the edge of the membrane does not depend on the elasticity constants of the membrane media [32]. Finally, both the radial deformation  $\Delta R_m = u(r = R)$ , the strain  $\frac{\Delta R_m}{R}(r = R)$  and the stress  $\sigma_{rm} = \sigma_{rr}(r = R)$  of the membrane edge are:

$$\Delta R_m = \frac{F_m (1 - \nu_m)}{t_m E_m} R, \quad (26)$$

$$\frac{\Delta R_m}{R} = \frac{F_m (1 - \nu_m)}{t_m E_m}, \quad (27)$$

$$\sigma_{rm} = \frac{F_m}{t_m}. \quad (28)$$

It is important to mention that all expressions in SubSection II.B are valid for a membrane of thickness  $t_m$  in the shape of a ring with concentric internal and external radii, subject to internal membrane clamping. This is still the same case of two-dimensional uniform expansion as considered above.

### C. Gas in toroidal shell

Consider the pressure of the gas in the toroidal shell. We describe the gas by the equation for the real gas. Therefore, we are not considering atoms or molecules of the gas as point particles that interact with

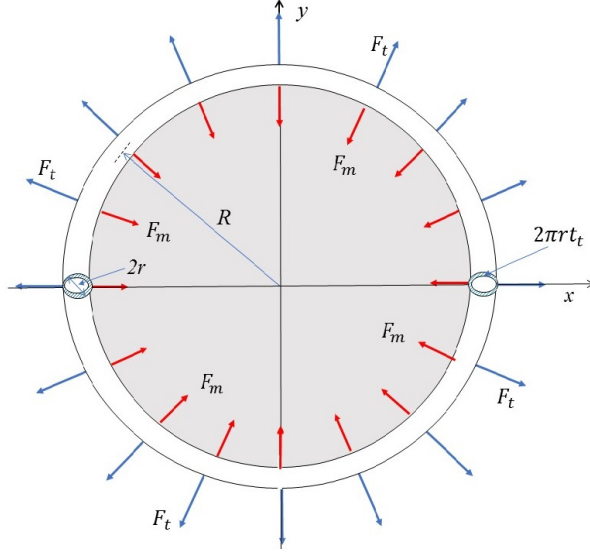


FIG. 5: (Color online) Schematics for the action of uniform radial forces  $F_t$  and  $F_m$  per unit of circumferential length on the toroidal shell. The force opposite in direction and equal in magnitude to  $F_m$  acts on the circular membrane and is not shown. For visibility, the cross-section of the toroidal shell is given in 3D format. The figure is not to scale:  $R \gg r$  and  $r \gg t_t$ .

toroidal shell only. We are taking into account the volume that a real gas atoms or molecules take up and gas atoms or molecules interaction with each other that are experiencing an attraction at low pressure and repulsion at high pressure. The corresponding van der Waals equation of state reads

$$\left(P + a \frac{n^2}{V^2}\right) (V - nb) = nR_g T. \quad (29)$$

In Eq. (29)  $a$  and  $b$  are the gas dependent constants,  $n = \frac{M_g}{\mu}$  is the number of moles of the gas, where  $M_g$  is the mass of the gas not considering diffusion losses and  $\mu$  is the molar weight of the gas,  $V$  and  $T$  are volume and temperature of the gas, respectively, and  $R_g = 8.31 \text{ J}\cdot\text{K}^{-1}\text{mol}^{-1}$  is a universal gas constant. We assume that at equilibrium the pressure of the gas in the toroidal shell obeys to the isochoric process because it is confined in the interior volume  $V = 2\pi^2 r^2 R$ , which only slightly changes because of the increase of the torus radius by  $\Delta R_t$  (7) due to the gas pressure. For the torus with large aspect ratio this increase of the volume can be neglected. The internal pressure produces the forces that remain normal to the surface. As it follows from Eq. (29) for the isochoric process the pressure

$$P = n \frac{R_g T}{2\pi^2 r^2 R - nb} - n^2 \frac{a}{4\pi^4 r^4 R^2}. \quad (30)$$

As it follows from Eq. (30) the pressure of the confined gas is defined by its mass, temperature, the gas parameters  $a$  and  $b$ , and the characteristic size of the torus radii  $R$  and  $r$ .

Using Eqs. (4) and (30) one can find the in-plane tensile force per unit length in the membrane produced by the inflatable torus shell filled with a gas

$$F_t = n \frac{\pi r^2 R_g T}{2\pi^2 r^2 R^2 - nbR} - n^2 \frac{a}{4\pi^3 r^2 R^3}. \quad (31)$$

#### D. Circular membrane attached to toroidal shell

In the absence of the gas, there are no stresses along the line of the attachment of the membrane to the toroidal shell. The gas in the toroidal shell causes the force  $F_t$  acting on the toroidal shell radially out and  $F_m$  acting on the toroidal shell from the membrane radially in as shown in Fig. 5. The latter force

is in return to the stress caused by the force of the toroidal shell on the membrane equal in magnitude to  $F_m$ . In the state of equilibrium we have

$$\Delta R_t = \Delta R_m. \quad (32)$$

The radial forces  $F_t$  and  $F_m$  result in total radial force  $F_t - F_m$ , which has to be balanced by the elastic forces in the toroidal shell causing the shell radius change  $\Delta R_t$  according to (7). However, the force  $F_t$  in (7) for stand-alone toroidal shell should be replaced by the force  $F_t - F_m$  for the toroidal shell and membrane combination. Using (7) in place of  $\Delta R_t$  with  $F_t$  replaced to  $F_t - F_m$ , and using (26) for the  $\Delta R_m$  of membrane leads (32) to

$$\frac{(F_t - F_m)R^2}{2\pi r t_t E_s} = \frac{F_m}{t_m} \frac{(1 - \nu_m)}{E_m} R, \quad (33)$$

and

$$F_m = F_t \left( 1 + 2\pi \frac{r}{R} \frac{t_t}{t_m} \frac{E_t}{E_m} (1 - \nu_m) \right)^{-1}. \quad (34)$$

Using (4) for  $F_t$  Eq. (34) can be rewritten as

$$F_m = \pi P \frac{r^2}{R} \left( 1 + 2\pi \frac{r}{R} \frac{t_t}{t_m} \frac{E_t}{E_m} (1 - \nu_m) \right)^{-1}, \quad (35)$$

where  $P$  is defined by (30).

In conclusion, (27) with (35) for  $F_m$  allow the determination of the strain of both the toroidal shell and the membrane. Equation (28) determines the radial pressure on the membrane edge, and (5) with  $F_t$  replaced by  $F_t - F_m$ :

$$\sigma_t = \frac{(F_t - F_m) R}{2\pi r t_t} \quad (36)$$

provides for the tensile stress of the toroidal shell for the system of the circular membrane attached to the toroidal shell.

### III. SAIL MEMBRANE

The sail surface is a circular membrane of radius  $R$  represents the "still" drum head shape under the tensile stress produced by the inflated toroidal shell. The boundary of the membrane is a circle of radius  $R$  centered at the origin and represents the rigid frame to which the membrane is attached. In the equilibrium position, the membrane is stretched and fixed along its entire boundary by the toroidal shell in the  $x - y$  plane. The tension per unit length  $F_m$  caused by stretching the membrane is the same at all points and in all directions and does not change during the motion.

When the deployment of the membrane ends it can experience the vibration. The mathematical equation that governs the normal transverse vibrations of the membrane is the wave equation with zero boundary conditions. The wave equation has been widely studied in the literature and is as follows:

$$\frac{\partial^2 \mathbf{u}}{\partial t^2} = c_s^2 \left( \frac{\partial^2 \mathbf{u}}{\partial x^2} + \frac{\partial^2 \mathbf{u}}{\partial y^2} \right), \quad c_s^2 = \frac{F_m}{\varkappa}, \quad (37)$$

where  $\mathbf{u}(x, y) = 0$  on the boundary of the membrane,  $\varkappa$  is the mass per area of the membrane, and  $c_s = \sqrt{\frac{F_m}{\varkappa}}$  is the sound speed. Equation (37) is the two-dimensional wave equation, which is a second order partial differential equation. Due to the circular geometry of the membrane, it is convenient to rewrite Eq. (37) using the cylindrical coordinates

$$\frac{\partial^2 \mathbf{u}}{\partial t^2} = c_s^2 \left( \frac{\partial^2 \mathbf{u}}{\partial \mathbf{r}^2} + \frac{1}{\mathbf{r}} \frac{\partial \mathbf{u}}{\partial \mathbf{r}} + \frac{1}{\mathbf{r}^2} \frac{\partial \mathbf{u}}{\partial \varphi} \right), \quad \text{for } 0 \leq \mathbf{r} < R, \text{ and } 0 \leq \varphi \leq 2\pi \quad (38)$$



with the boundary condition  $\mathbf{u}(\mathbf{r}, \varphi, t) = 0$  for  $\mathbf{r} = R$ , which means that the membrane is fixed along the boundary circle of the radius  $R$  in the  $x - y$ -plane for all times  $t \geq 0$ .

To determine solutions  $\mathbf{u}(\mathbf{r}, \varphi, t)$  that are radially symmetric, we solve Eq. (38) following the three standard steps: i. using the method of separation of variables, we first determine solutions as  $\mathbf{u}(\mathbf{r}, \varphi, t) = \mathfrak{U}(\mathbf{r}, \varphi)V(t)$  and obtain two independent differential equations for  $\mathfrak{U}(\mathbf{r}, \varphi)$  and  $V(t)$  functions; ii. from the solutions of those ordinary differential equations we determine solution (eigenfunctions)  $\mathfrak{U}(r, \varphi)$  which satisfy the boundary condition  $\mathfrak{U}(\mathbf{r}, \varphi) = 0$  for  $\mathbf{r} = R$  and find the corresponding eigenvalues. Then find the periodical solution  $V(t)$  by solving the second differential equation; iii. we compose these solutions and obtain the radially symmetric solution  $\mathbf{u}(\mathbf{r}, t)$  that satisfy the conditions  $\mathbf{u}(\mathbf{r}, 0)$  and  $\frac{\partial \mathbf{u}(\mathbf{r}, t)}{\partial t}$  depend only on  $\mathbf{r}$ . The corresponding method of a solution is given in Ref. [30]. In-plane vibrations and dumping of the transfer vibrations in particular due to the solar radiation pressure are out of the score of this study.

#### IV. RESULTS AND DISCUSSION

The theory presented in the previous sections provides expressions to calculate different quantities related to a torus-shaped solar sail such as stresses in the toroidal shell and membrane, the radial force that acts on the membrane and their dependence on the gas mass. The general assumptions of applicability of these expressions are the following:

- i. both strain and stress for the membrane and toroidal shell are small and within the limit of elasticity;
- ii. the radius of the membrane is much greater than the radius of the toroidal shell:  $R \gg r$ .
- iii. the material thickness of the membrane and toroidal shell are significantly smaller than the radius of the toroidal shell:  $t_m \ll r$  and  $t_t \ll r$ .

The first condition insures the mechanical stability of the sail and requires that the stress in the membrane and toroidal shell have to be less than the yield strength of the corresponding material. To satisfy the second condition the values of  $\frac{R}{r} \sim 10^2$  are used. To meet the third requirement the values  $\frac{t_m}{r} \approx \frac{t_t}{r} \sim 10^{-5}$  are considered. In our calculations we consider CP1 Polyimide film [35] as an example of the material of the membrane and toroidal shell (CP1 is planned to be used for the Solar Cruiser [36]) and the hydrogen as the filling gas. However, to meet the first condition the thickness of the toroidal shell is considered twofold as for the membrane. As it follows from Eqs. (4), (34), and (36) this leads almost twofold decrease of the shell stress. The properties of CP1, corresponding parameters and gas constants are listed in Table I. The yield strength of CP1 is not available to the authors. In general, it is much less than the Young modulus. Nonetheless, one can estimate the yield strength to be greater than  $\sim 10^{-2}$  part of the Young modulus, keeping in mind that the real design decisions have to be based on experimentally measured values.

One of the key metrics related to the performance of solar sail is the characteristic acceleration [2–4]. The characteristic acceleration is defined as  $a_0 = 2\eta P_0/\chi$ , where  $0.5 \leq \eta \leq 1$ ,  $P_0$  is the solar radiation pressure near the Earth and  $\chi = M/A$  is the areal density. In the latter expression,  $M$  is the total mass of the torus-shaped solar sail defined by Eq. (8) and  $A$  is the sail membrane area. It is worth mentioning that we neglect the projectional area of the toroidal shell:  $4\pi r(R + r) \ll \pi R^2$ . However, consideration of this area only decreases the areal density. While the actual sail acceleration is a function of heliocentric distance and its orientation, the characteristic acceleration allows a comparison of solar sail design concepts on an equal footing. The areal density  $\chi$  is an important parameter determining the sail acceleration due to electromagnetic radiation pressure. It is easy to calculate  $\chi$  for known geometry and densities of sail materials. Less  $\chi$  leads to the greater sail acceleration. The dependence of the areal

TABLE I: Model parameters for the sail membrane and hydrogen gas.  $\rho_m$ ,  $E_m$ ,  $\nu_m$  and  $t_m$  are the density, Young modulus, Poisson ratio and thickness of the sail membrane, respectively.

Sail's membrane, CP1				Gas parameters		
$\rho_m$ , kg/m <sup>3</sup>	$E_m$ , Pa	$\nu_m$	$t_m$ , m	$\mu$ , g/mol	$a$ , L <sup>2</sup> bar/mol <sup>2</sup>	$b$ , L/mol
$1.43 \times 10^3$	$2.17 \times 10^9$	$3.40 \times 10^{-1}$	$3.5 \times 10^{-6}$	2.0159	0.2476	0.02661

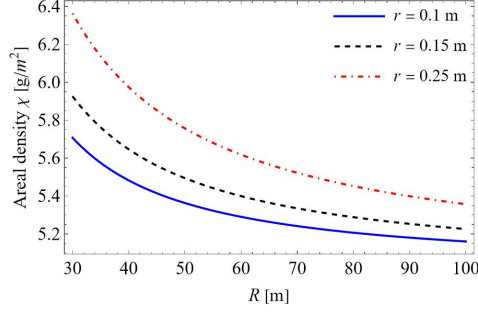


FIG. 6: (Color online) The dependence of the areal density the solar sail on the membrane radius for different radii of the toroidal shell.

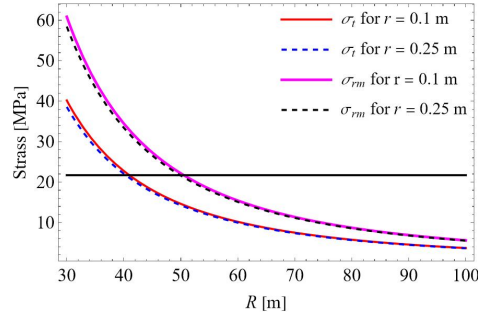


FIG. 7: (Color online) The dependence of the tensile stress of the toroidal shell  $\sigma_t$  and the membrane radial stress  $\sigma_{rm}$  on the membrane radius for different radii of the toroidal shell. The horizontal line corresponds to  $10^{-2}E_m$  MPa. Calculations performed for the gas mass  $M_g = 0.750$  kg.

density of the solar sail on the membrane radius for different radii of the toroidal shell is shown in Fig. 6. As is expected the areal density increases with the increase of the toroidal shell radius and decrease of the sail membrane radius. When the membrane radius increases from 30 m to 100 m the areal density decreases from  $\sim 6.4$  g/m<sup>2</sup> to  $\sim 5.2$  g/m<sup>2</sup>. While the dependence of  $\chi$  on the toroidal shell radius is important, the mass of the gas has negligible contribution.

The expressions (28) and (36) are used to calculate the radial stress of the membrane and tensile stress of the toroidal shell. Analysis of these expressions shows the strong dependence on the membrane radius and on the pressure of the gas, but negligible dependence on the radius of the toroidal shell. Results of calculations performed for the different fixed radii of the toroidal shell are presented in Fig. 7. The both stresses decrease with the increase of membrane radius and the results show that for any given radius the membrane stress is greater than respective toroidal shell stress. Thus, the stability of the membrane will insure the stability of the entire shell-membrane structure. The membrane stress stays within  $10^{-2}E_m$ . The crossover points radii represent the lower limits of the sail radii.

In Eq. (30) the second term is small and one can say that the gas pressure in the toroidal shell is approximately directly proportional to the gas mass. Therefore, analysis of Eqs. (31) and (34) shows that the force  $F_t$  per unit length of the toroidal shell and the force  $F_m$  per unit length of the membrane also are approximately directly proportional to the gas mass. The same strong dependence on the gas mass along with the strong dependence on the membrane radius is reflected on both the toroidal shell and membrane stresses. The results presented in Fig. 8 show the dependence of the membrane stress on the membrane radius for different masses of the gas. The strong dependence of the radii of the crossover points on the gas mass is obvious. The stable sails need to have radii greater than the radii of crossover points in Fig. 8.

The logical question which arises now is the following: which value of the sail radius should be considered to deploy the sail successfully? Although a certain answer can be obtained only in the experiment

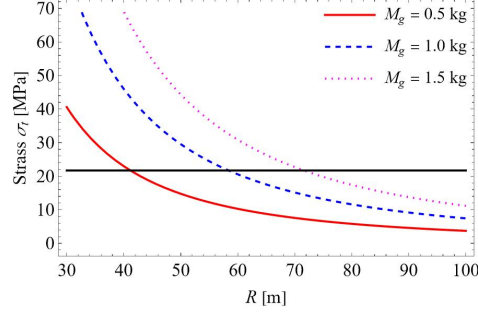


FIG. 8: (Color online) The dependence of the membrane radial stress  $\sigma_{rm}$  on the membrane radius for different masses of the gas in the toroidal shell. The horizontal line corresponds to  $10^{-2}E_m$  MPa. Calculations performed for  $r = 0.1$  m.

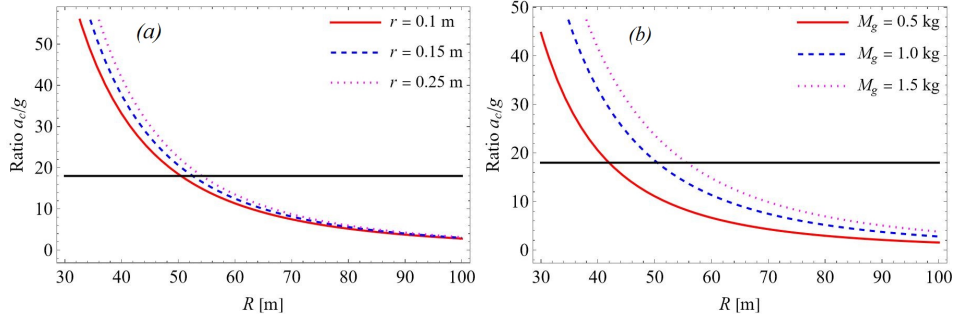


FIG. 9: (Color online) The dependence of the ratio  $a_c/g$  on the radius of the solar sail membrane for (a) different radii of the toroidal shell for  $M_g = 1.0$  kg and (b) different masses of the gas in the toroidal shell for  $r = 0.1$  m. The horizontal line for the ratio  $a_c/g$  is obtained based on the result from Ref. [7].

it is possible to make some estimations by introducing the ratio  $a_c/g$  given as

$$\frac{a_c}{g} = \frac{(F_t - F_m)}{g(2\pi r t_t \rho_t + M_g/2\pi R)}, \quad (39)$$

where  $g = 9.8 \text{ m/s}^2$  is the acceleration due to gravity at the Earth surface. The quantity  $a_c$  is effective acceleration equivalent to centripetal acceleration of the shell would it be spinning around its center with frequency

$$f = \frac{1}{2\pi} \left( \frac{a_c}{R} \right)^{1/2}. \quad (40)$$

The greater  $a_c/g$  ratio the greater the chance of successful deployment of initially folded toroidal shell and sail membrane to the open state of circular shape. A simple analysis of the partial derivatives shows that  $\sigma_t$ ,  $\sigma_{rm}$ , and  $a_c/g$  are the monotonically decreasing functions of the membrane radius  $R$ , radius  $r$  of the toroidal shell cross-section and increasing functions of the gas mass.

We compare the calculated values of  $a_c/g$  ratio with the equivalent estimate based on the successful ground demonstration of the spinning sail deployment by Jet Propulsion Laboratory [7]. The data provided in Ref. [7] for the spinning frequency 200 RPM or more of the sail of 0.8 m in diameter gives the estimate of the ratio of centripetal acceleration over the acceleration due to gravity equal to 18 or more. The calculated  $a_c/g$  ratio is presented in Fig. 9. It is evident from Fig. 9a that the dependence of the ratio on the toroidal shell radius  $r$  is fairly weak and similar to the dependence of the stresses on  $r$  - see Fig. 7. Thus, the choice of lower  $r$  is preferable for the sail due to the less arial density. Our choice for toroidal radius  $r$  is 0.1 m. Results presented in Fig. 9b show strong dependence of the  $a_c/g$  ratio on the gas mass. The radii of the crossover points of the  $a_c/g$  versus  $R$  curves with the horizontal line at  $a_c/g = 18$  represent the upper limits of the sail radius. The sail with radius less than these upper limits is expected to successfully deploy into a circular shape. In summary, there are two limits for the radii of

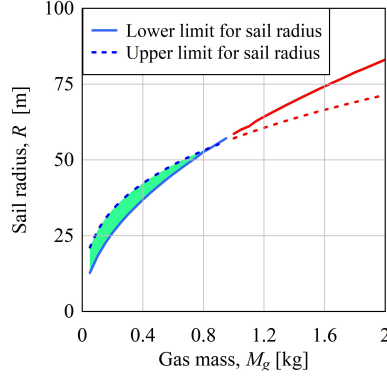


FIG. 10: (Color online) Limitations for the radius of the sail. The colored area shows the allowed radii of the sail's membrane for the radius of the toroidal shell  $r = 0.1$  m.

the sail: i. the lower limit is due to the sail stability requirement demanding the stresses to be within limits of elasticity; ii. the upper limit is due to requirement of the successful deployment. The radius of the sail has to simultaneously satisfy both requirements being greater than the lower limit and less than the upper limit. This means that the lower limit has to be less than the upper limit. The dependence of the limits of the toroidal shell-membrane radii on the gas mass for choice of  $r = 0.1$  m is presented in Fig. 10. This is kind of a solar sail phase diagram. The coordinates of the crossover point are:  $R = 54.5$  m and  $M_g = 0.870$  kg. The sails with the radius and the gas mass within the area laying to the left of the crossover point and defined at the top by the upper limit and at the bottom by the lower limit curves are deployable and stable. The sails with the radius and gas mass to the right of the crossover point are either unstable and/or not deployable. For example, in the case of CP1 Polyimide film the sail membrane of  $R = 51$  m attached to the toroidal shell of  $r = 0.1$  m inflated by 0.75 kg of the hydrogen is the optimal fit. The same kind of the diagram can be calculated for other choices of toroidal shell radius  $r$ . The location shift of the crossover point with the variation of  $r$  from 0.1 m to 0.25 m is quit small, within 1.5 m and 60 g.

For a sail with  $R = 51$  m and inflatable toroidal shell with  $r = 0.1$  m,  $M_g = 0.750$  kg of the gas in the toroidal shell and for the tension of the membrane given by Eq. (35) we calculated the first three normal transverse vibration modes of the deployed and stretched circular sail. For this tension and the corresponding geometric characteristics of the membrane, the maximum deviation of the solar sail membrane was found. The results of these calculations are shown in Fig. 11. Each graph corresponds to the instant of time when the maximum deviation of the membrane from its equilibrium position is reached. Our results show that the total deviations of the membrane from the equilibrium position with free modes of oscillations will not exceed a few millimeters and the maximal deviation is observed for the first mode. However, one should mention that these vibrations are related to the static deployed sail and only are transverse or out of plane without taking into account any damping in particular the dumping due to radiation pressure. These results could dramatically change when one considers the vibration during the dynamics of opening the sail when the gas is inserting into the toroidal shell. This aspect along with the in-plane vibrations and dumping is out of the scope of this paper and will be considered

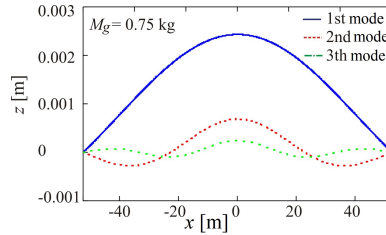


FIG. 11: (Color online) Dynamics of the vibrating membrane. Maximum membrane deviations for the first (0,1), second (0,2) and third (0,3) modes of normal oscillations.

somewhere later.

## V. CONCLUSIONS

In this article we present the theoretical study of the circular solar sail with inflatable torus-shaped shell. In the framework of a strict mathematical approach based on classical theory of elasticity we justify an idea of the deployment and stretching of the solar sail membrane attached to the inflatable toroidal shell. We obtained the analytical expressions that can be applied to a wide range of materials for both the shell and sail membrane. The presented numerical example demonstrates the ability of the developed theory to provide sound estimates of the stresses of the inflatable shell and the solar sail membrane solely based on the geometry, gas mass and elastic properties of the materials. Analysis of these expressions shows the strong dependence of stresses and strains on the membrane radius and on the pressure of the filled gas, but negligible dependence on the radius of the toroidal shell. We performed numerical calculations for the sail of radius of 30 to 100 m made of CP1 membrane and attached to the toroidal shell of the same material with the varied cross-section radius and gas mass. We predict that by introducing the gas into the inflatable toroidal rim one can deploy and stretch circular solar sail membrane up to 54 m of radius. It is worth noting that the same calculations can be easily performed for the other suggested materials for a solar sail such as Kapton or aluminized Mylar or others [37]. It is shown that the normal out of plane vibrations of the sail membrane under tension caused by gas pressure are negligible.

To conclude, our theoretical approach and calculations demonstrate the feasibility of deployment and stretching of the solar sail constructed as a thin circular membrane attached to the inflatable toroidal shell. At this point, an experimental research is necessary to find out the level of feasibility of such a solar sail for future exploration of the solar system and beyond by mean of the electromagnetic pressure propellant.

- 
- [1] E. N. Polyakhova, *Kosmicheskii Polet s Solnechnim Parusom (Space Solar Sailing) (in Russian)* Moscow, Nauka, 1986.
  - [2] C. R. McInnes, *Solar Sailing - Technology, Dynamics and Mission Applications*. Springer, Praxis Publishing, Chichester, 1999.
  - [3] G. L. Matloff, *Deep Space Probes: To the Outer Solar System and Beyond*. Springer/Praxis Books, 2005.
  - [4] G. Vulpetti, L. Johnson, G. L. Matloff, *Solar Sails - A Novel Approach to Interplanetary Travel*. Copernicus Books, 2008.
  - [5] J. M. Fernandez, V. J. Lappas, A. J. Daton-Lovett, Completely stripped solar sail concept using bi-stable reeled composite booms. *Acta Astronautica* **69**, 78–85 (2011).
  - [6] G. Genta and E. Brusa, The parachute sail with hydrostatic beam: a new concept for solar sailing. *Acta Astronautica* **44**, 133–140 (1999).
  - [7] M. Salama, C. White, and R. Leland, Ground demonstration of a spinning solar sail deployment concept. *J. Spacecraft Rock.* **40**, 9–14 (2003) <https://doi.org/10.2514/2.3933>.
  - [8] J. M. Fernandez, Advanced deployable shell-based composite booms for small satellite structural applications including solar sails, Corpus ID: 114881473, Engineering (2017).
  - [9] J. M. Fernandez, G. K. Rose, C. J. Younger, G. D. Dean, J. E. Warren, O. R. Stohlman, and W. Wilkie, NASA’s advanced solar sail propulsion system for low-cost deep space exploration and science missions that uses high performance rollable composite booms, Corpus ID: 113546105, Physics (2017).
  - [10] M. B. Quadrelli and J. West, Sensitivity studies of the deployment of a square inflatable solar sail with vanes, *Acta Astronautica* **65**, 1007–1027 (2009).
  - [11] J. M. Fernandez, L. Visagie, M. Schenk, O. R. Stohlman, G. S. Aglietti, V. J. Lappas, and S. Erb, Design and development of a gossamer sail system for deorbiting in low earth orbit. *Acta Astronautica —textbf103*, 204–225 (2014). doi:10.1016/J.ACTAASTRO.2014.06.018
  - [12] A. Boschetto, L. Bottini, G. Costanza, and M. E. Tata, Shape memory activated self-deployable solar sails: small-scale prototypes manufacturing and planarity analysis by 3D laser scanner, *Actuators* **8**, 38 (2019).
  - [13] A. Boschetto, L. Bottini, G. Costanza, and M. E. Tata, A novel self-deployable solar sail system activated by shape memory alloys, *Aerospace* **6**, 78 (2019).
  - [14] B. Vatankhahghadim and C. J. Damaren, Solar sail deployment dynamics, *Adv. Space Res.* **67**, 2746–2756 (2021).

- [15] V. Parque, W. Suzaki, S. Miura, A. Torisaka, T. Miyashita, and M. Natori, Packaging of thick membranes using a multi-spiral folding approach: Flat and curved surfaces, *Adv. Space Res.* **67**, 2589–2612 (2021).
- [16] L. T. Hibbert and H. W. Jordaan, Considerations in the design and deployment of flexible booms for a solar sail, *Adv. Space Res.* **67**, 2716–2726 (2021).
- [17] V. Ya. Kezerashvili and R. Ya. Kezerashvili, On deployment of solar sail with superconducting current-carrying wire, *Acta Astronautica* **189**, 196–198 (2021).
- [18] V. Ya. Kezerashvili and R. Ya. Kezerashvili, Solar sail with superconducting circular current-carrying wire, *Adv. Space Res.* **69**, 664–676 (2022).
- [19] G. F. Pezditz, Erectable space structures-ECHO Satellites, NASA N62-12545, 1962.
- [20] D. Cadogan, J. Stein, and M. Grahne, Inflatable composite habitat structures for lunar and mars exploration, *Acta Astronautica*, **44**, 399–406 (1999).
- [21] J. Strobl, The hollow-body solar sail, *JBIS*, **42**, 515–520 (1989).
- [22] D. Hayn, The orbital torus solar sail vehicle (ORTOSS: Orbitaler Torus Sonnensegler), *Luft und Raumfahrt*, **11**, 34–36 (1990).
- [23] R. E. Freeland, G. D. Bilyeu, G. R. Veal, M. D. Steiner, and D. E. Carson, Large Inflatable Deployable Antenna Flight Experiment Results, *Acta Astronautica*, **41**, 267–277 (1997).
- [24] J. Strobl, The hollow-body solar sail as a transporter of a Radio Telescope, *JBIS* **47**, 67–70 (1994).
- [25] L. M. Leigh and M. L. Tinker, Dynamic characterization of an inflatable concentrator for solar thermal propulsion, *J. Spacecraft and Rocket*, **40**, 24–27 (2003).
- [26] K. B. Smalley, M. L. Tinker, and W. S. Taylor, Structural modeling of a five-meter thin-film inflatable antenna/concentrator, *J. Spacecraft and Rocket*, **40**, 27–29 (2003).
- [27] G. L. Matloff, The beryllium hollow-body solar sail and interstellar travel, *JBIS* **59** 349–354 (2006).
- [28] R. Ya. Kezerashvili and G. L. Matloff, Solar radiation and the beryllium hollow-body sail: 1. The ionization and disintegration effects, *JBIS* **60**, 169–179 (2007).
- [29] R. Ya. Kezerashvili and G. L. Matloff, Solar radiation and the beryllium hollow-body sail: 2. Diffusion, recombination and erosion processes, *JBIS* **61** 47–57 (2008).
- [30] R. Ya. Kezerashvili, O. L. Starinova, A. S. Chekashov, and D. J. Slocki, A torus-shaped solar sail accelerated via thermal desorption of coating, *Adv. Space Res.* **67**, 2577–2588 (2021).
- [31] S. Timoshenko and J. N. Goodier, *Theory of Elasticity*, 2<sup>nd</sup> Edition, McGraw-Hill Book Com., New York, USA, 1951.
- [32] L. D. Landau and E. M. Lifshitz, *Theory of Elasticity*, 3<sup>rd</sup> English Edition, Revised and Enlarged, Pergamon Press, Oxford, UK, 1986.
- [33] H. Kraus, *Thin Elastic Shells*. Wiley, New York 1967.
- [34] A. D. Polyanin and V. F. Zaitsev, *Handbook of Ordinary Differential Equations*, CRC Press, Taylor & Francis, Boca Raton, USA, 2018.
- [35] A. Peloni, D. Barbera, S. Laurenzi, C. Circi, Dynamic and structural performances of a new sailcraft concept for interplanetary missions, *Scientific World Journal*, Volume 2015, Article ID 714371, 14 pages <http://dx.doi.org/10.1155/2015/714371>.
- [36] Les Johnson, Privet communication.
- [37] G. L. Matloff and R. Ya. Kezerashvili, Interstellar solar sailing: a figure of merit for monolayer sail, *JBIS* **61**, 330–333 (2008).